Journal of Herpetology, Vol. 54, No. 4, 446–459, 2020

A New Species of New Guinea Worm-Eating Snake (Elapidae: *Toxicocalamus* Boulenger, 1896), with Comments on Postfrontal Bone Variation Based on Micro-computed Tomography

JACKSON R. ROBERTS[1,2,3] AND CHRISTOPHER C. AUSTIN[1,2]

[1]*Division of Herpetology, Museum of Natural Science, Louisiana State University, Baton Rouge, Louisiana, 70803, USA*
[2]*Department of Biological Sciences, Louisiana State University, Baton Rouge, Louisiana, 70803, USA*

ABSTRACT.—**Morphology and DNA sequences are used to describe a new species of New Guinea Worm-Eating Snake (Elapidae: *Toxicocalamus* Boulenger, 1896) from Papua New Guinea: *Toxicocalamus goodenoughensis* n. sp., endemic to Goodenough Island of the D'Entrecasteaux Archipelago. *Toxicocalamus goodenoughensis* morphologically most closely resembles *T. pachysomus* Kraus, 2009, but it differs by having undivided nasal scales completely surrounding nares (vs. divided), pale yellow markings on supralabials (vs. purple), a yellow nape band (vs. unbanded uniform nape), a dark gray-brown dorsum (vs. medium brown), dark brown mottling on yellow ventral scales, darkening toward cloaca (vs. uniform light brown), and >175 ventral scales. Phylogenetically, *T. goodenoughensis* is sister to another D'Entrecasteaux endemic, *T. nigrescens* Kraus, 2017. Coalescent-based species delimitation found the new species to be uniquely delimited from all other taxa ($n = 13$) in all combinations of parameters settings. Micro-computed tomography (μCT) scanning revealed the presence of distinctive variation in postfrontal bone morphologies, with three morphotypes exhibited within the genus: directed forward, directed lateral/perpendicular to cranium, and absent. *Toxicocalamus goodenoughensis* was found to have a sickle-shaped and directed forward postfrontal bone. The directed forward morphotype was shared by *T. loriae* clade 3 (sensu Strickland et al., 2016), *T. mintoni*, *T. nigrescens*, and *T. pachysomus*. Our work is the most comprehensive phylogenetic analysis of the genus and the first study using μCT scanning for comparative morphology of *Toxicocalamus*. We also provide an updated dichotomous key for the genus.**

New Guinea is one of the world's top five high biodiversity wilderness areas because of a high percentage of intact wilderness coupled with extremely high vertebrate biodiversity (Mittermeier et al., 2003). Much of the diversity found on the island comprises endemic taxa with all congeners being found only on the island or adjacent associated islands (Allison, 1996; Mittermeier et al., 2003). With respect to herpetofauna, New Guinea hosts more than 512 species of amphibians and reptiles, with ~75% endemic to New Guinea (Allison, 1996; O'Shea, 1996; Menzies, 2006). The pattern of high endemism and accelerated speciation derives in part from the unique and complex tectonic history of the island during the Miocene. Most recently, in the middle-to-late Miocene (~12–6 million years ago [mya]), collision and shearing between the Australian (southern half of New Guinea) and Pacific (northern half) plates have created the central mountain range that divides the northern and southern portions of the island, causing separation and isolation and leading to allopatric speciation (Hall, 2002; van Ufford and Cloos, 2005; Baldwin et al., 2012). Significant changes in topographic and subaerial landscape occurred not just on the mainland but also in the seas surrounding New Guinea, specifically off the southeastern coast of New Guinea. The late Miocene (~6 mya) saw the formation of the Woodlark Basin, and the complex tectonics responsible for the Woodlark Basin coupled with rising sea levels formed many of the southeastern Papuan archipelagos: Louisiade, Trobriand, and Woodlark (Taylor et al., 1995; Webb et al., 2014). The D'Entrecasteaux Archipelago, however, is in fact a product of metamorphic core complex uplifting, making this island chain unique in its originating process (Little et al., 2011; Baldwin et al., 2012). Many of these archipelagos host endemic taxa closely related to congeners on the New Guinea mainland (Malnate and Underwood, 1988; Kraus and Allison, 2004, 2006, 2007; Metzger et al., 2010; Kraus, 2017a; Ruane et al., 2018). The New Guinea Worm-Eating Snakes of the genus *Toxicocalamus* Boulenger, 1896 represent one of these unique lineages.

Toxicocalamus are semifossorial elapids within the Hydrophiinae and are found exclusively on New Guinea and its peripheral islands (O'Shea, 1996; Kraus, 2009, 2017b; O'Shea et al., 2015, 2018). Previous workers have found that sea snakes (*Laticauda* spp.) are the sister taxa to all other hydrophiines (Keogh, 1998; Scanlon and Lee, 2004; Sanders et al., 2008; Metzger et al., 2010; Lane and Shine, 2011; Strickland et al., 2016) and, even more recently, have shown *Toxicocalamus* to be monophyletic and an early-branching lineage within the hydrophiines (Strickland et al., 2016). Unlike some of its highly venomous relatives within Hydrophiinae, *Toxicocalamus* are small snakes (with a few exceptions, i.e., *T. ernstmayri* and *T. grandis* reach roughly 1 m in length) that show no inclinations to strike for self-defense (Kraus, 2017b), despite possessing toxic venom (Calvete et al., 2012).

Toxicocalamus currently comprises 15 described species, of which 9 are found on the mainland of New Guinea and 6 are endemic to the southeastern islands of the D'Entrecasteaux, Louisiade, and Woodlark archipelagos (McDowell, 1969; O'Shea, 1996; Kraus, 2009, 2017b; O'Shea et al., 2015, 2018). Ecological and natural history data are limited for this group, mostly because of their secretive fossorial lifestyles (O'Shea, 1996). Despite observational difficulties imposed by their subterranean habits, researchers have reported species of *Toxicocalamus* to be primarily vermivorous (eating mostly earthworms; O'Shea, 1996; Shine and Keogh, 1996; O'Shea et al., 2015; Austin, pers. obs.), with fly pupae and a land snail also having been reported from stomach contents (Bogert and Matalas, 1945; McDowell, 1969). Although our understanding of the ecology and natural history of these snakes is limited, there has been a recent surge in alpha taxonomic work, with six new species described in the last decade from newly collected

[3]Corresponding Author. E-mail: jrob265@lsu.edu
DOI: 10.1670/20-043

specimens and those long-held in collections (Kraus, 2009, 2017b; O'Shea et al., 2015, 2018).

Before 2009, the most recent taxonomic assessment of this group was completed by McDowell (1969) in a work comprising three species descriptions and a complete revision of the genus. Since McDowell's assessment, one molecular-based phylogeny has been produced by Strickland et al. (2016). Using seven loci (three mitochondrial and four nuclear), these authors showed additional evidence for Hydrophiinae monophyly; evidence for *Toxicocalamus* monophyly; and evidence of a polyphyletic *Toxicocalamus loriae* (Boulenger, 1898), a species that comprised six lineages of which now four are undescribed. The six *T. loriae* lineages identified were named clades 1–6, with *T. loriae* clade 1 representing what is thought to be true *T. loriae* and Fred Kraus describing *T. loriae* clade 5 as *T. nigrescens* Kraus, 2017 (Boulenger, 1898; Strickland et al., 2016; Kraus, 2017b).

A field expedition to Goodenough Island of the D'Entrecasteaux Archipelago (Milne Bay Province) in 2012 resulted in the collection of *Toxicocalamus* specimens that were diagnosable morphologically and genetically from all other species of the genus. Below, we describe the species, include it in the most comprehensive phylogenetic analysis of the genus to date, provide an updated dichotomous key for the genus, and include the first characterizations of any species of the genus by using micro-computed tomography (μCT) scanning.

Materials and Methods

Collection and Morphological Data.—Specimens were collected on a field expedition to Papua New Guinea in 2012 (Fig. 1), photographed in life (Fig. 2), and assigned a unique field tag number (CCA). In addition, tissue samples were taken for molecular analyses and whole specimens were prepared using standard techniques (Simmons, 2015). All collected specimens have been deposited in the Louisiana State University Museum of Natural Sciences (LSUMZ), and a list of examined specimens can be found in Appendix 1. Museum collection abbreviations follow Sabaj (2016).

Whole specimens were compared using traditional external morphological characters for snakes, including scale counts, scale patterns, and snout–vent length (SVL). Ventral scales were counted according to Dowling (1951) and excluded cloacal plate. Dorsal and subcaudal scales were counted following McDowell (1969). All measurements are taken in millimeters and reported to the first decimal as executed previously in recent *Toxicocalamus* descriptions (Kraus, 2017b; O'Shea et al., 2018). Species descriptions follow the format and organization presented by Kraus (2017b) where applicable. Following McDowell (1969), roman numerals indicate the number of grooved maxillary fangs innervating the venom gland.

Osteological characterizations were made with μCT scanning using a GE V|Tome|X M 240 scanner housed at the Nanoscale Research Facility at the University of Florida as well as a Nikon XTH 225 ST system housed at the Shared Materials Instrumentation Facility at Duke University. Reconstructed scans were visualized and segmented at LSUMZ by using Avizo v.9.5.0 (Thermo Fisher Scientific). Generated μCT scans have been made public through deposition on Morphosource.

Gene Sequencing.—We extracted DNA from newly collected tissues ($n = 3$) by using a standard salt extraction protocol (Austin et al., 2010). Four loci were sequenced to place the two new species within a previously published phylogenetic assessment of *Toxicocalamus* (Strickland et al., 2016): the two mitochondrial loci cytochrome *b* and *16S* and the two nuclear loci *c-mos* and *RAG-1*. Primers and relevant references can be found in Table 1. Final polymerase chain reaction products were sequenced using the Louisiana State University Genomics Facility. Sequences were trimmed and assembled using Geneious (Kearse et al., 2012). Alignments for phylogenetic analyses were made using MUSCLE under its default settings (Edgar, 2004). All new sequences have been deposited in GenBank (Table 2).

Species Included in Phylogenetic Analyses.—In addition to the newly collected specimens, our phylogenetic dataset comprised previously deposited sequence data for 9 nominal *Toxicocalamus* species: *T. holopelturus* McDowell, 1969, *T. longissimus* Boulenger, 1896, *T. loriae*, *T. mintoni* Kraus, 2009, *T. misimae* McDowell, 1969, *T. nigrescens* Kraus, 2017 (formerly *T. loriae* clade 5 sensu Strickland et al., 2016), *T. pachysomus* Kraus 2009, *T. preussi* (Sternfeld, 1913), and *T. stanleyanus* Boulenger, 1903, and 4 undescribed cryptic lineages—*T. loriae* clades 2, 3, 4, and 6 (Strickland et al., 2016). Six species were not included because of the lack of any known frozen or ethanol-preserved tissue: *T. buergersi* (Sternfeld, 1913), *T. cratermontanus* Kraus, 2017, *T. ernstmayri* O'Shea, Parker, and Kaiser, 2015, *T. grandis* (Boulenger, 1914), *T. pumehanae* O'Shea, Allison, and Kaiser, 2018, and *T. spilolepidotus* McDowell, 1969.

Phylogenetic Analyses.—To infer interspecific relationships within *Toxicocalamus*, we ran separate analyses using Bayesian inference and maximum likelihood algorithms. Before applying phylogenetic inferences, we determined optimal partitions and substitution models using PartitionFinder2 v.2.1.1 (Lanfear et al., 2017). We ran PartitionFinder2 with unlinked branch lengths, Bayesian information criterion model selection, and a set of user-specified partition models: by gene, by each position, concatenated, by genome, by genome plus *cytb* by itself, by gene and by codon, and by codon. We performed these steps with PartitionFinder2 for a concatenated sequence alignment, a nuclear sequence alignment (*c-mos* and *RAG-1*), and a mitochondrial sequence alignment (*cytb* and *16S*). PartitionFinder2 identified the ideal partition to be "by genome" for the concatenated dataset and "concatenated" for both the mitochondrial and nuclear analyses when analyzed separately. Model of nucleotide substitutions selected by PartitionFinder2 were GTR+I+G and HKY+G for the mitochondrial and nuclear genomes, respectively. For Bayesian inference, we used MrBayes v.3.2.7 (Ronquist and Huelsenbeck, 2003). Each MrBayes analysis included four runs and four chains and was run for 5,000,000 generations with a burn-in of 25%, with trees being sampled every 500 generations. For maximum likelihood analyses, we ran RAxML v.8.2.12 (Stamatakis, 2014). All RAxML analyses were run with the autoMRE setting with the GTRGAMMAI substitution model. The autoMRE flag executes a maximum of 1,000 bootstraps but terminates if convergence is detected before reaching the maximum. For this study, RAxML analyses converged at 200, 600, and 700 bootstrap replicates for the concatenated, mitochondrial, and nuclear alignments, respectively. Stationarity was also confirmed using Tracer v.1.7.1 (Rambaut et al., 2018). PartitionFinder2, MrBayes, and RaxML runs were executed using the CIPRES Science Gateway v.3.3.

Coalescent Species Delimitation.—In addition to morphological and phylogenetic assessments, we also delimited lineages by using the multispecies coalescent (MSC). To do this, we implemented Bayesian phylogenetics and phylogeography (BPP) v.4.1.4 (Flouri et al., 2018). BPP is a Bayesian Markov chain Monte Carlo (MCMC) program that can use multiple loci from multiple closely related species to perform both species

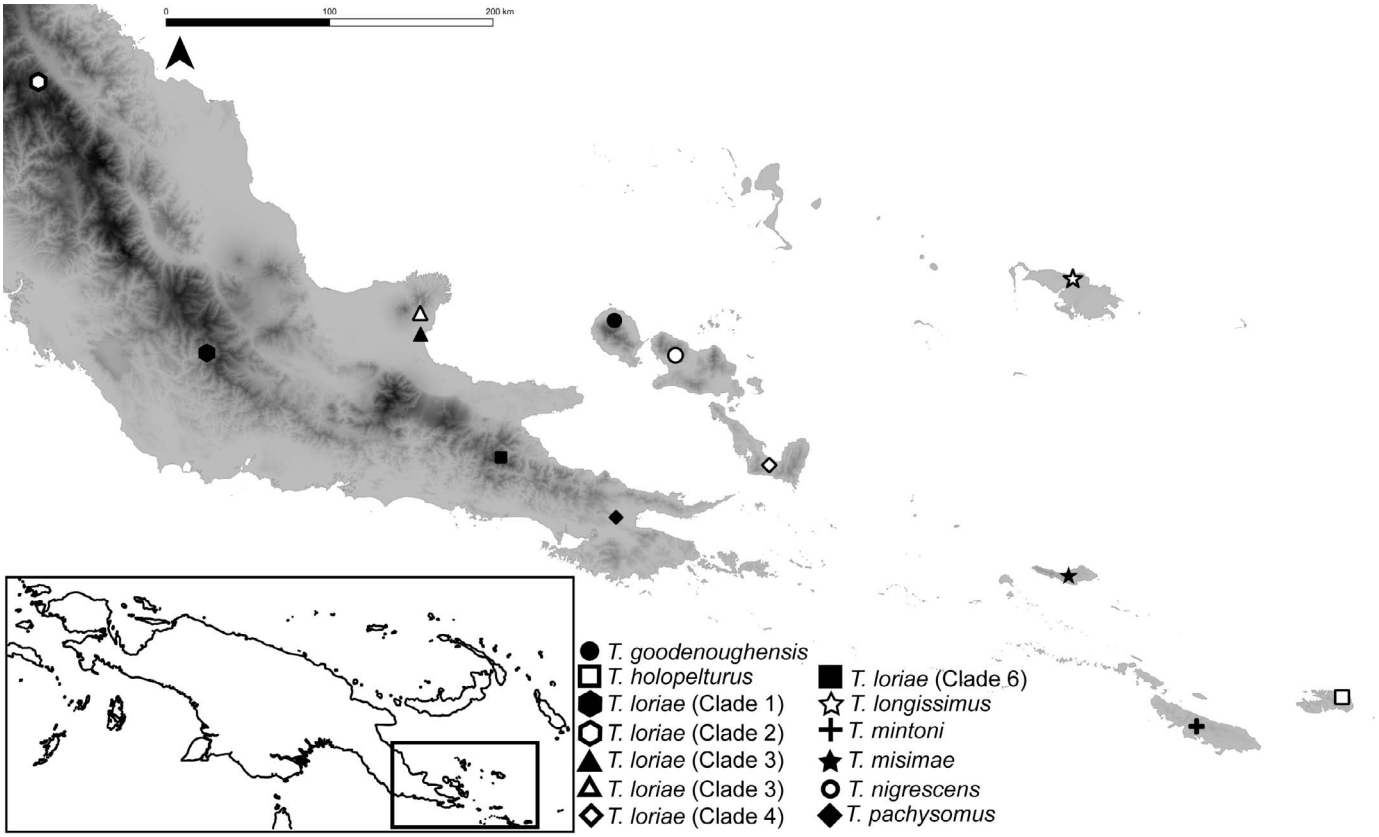

FIG. 1. Map showing southeast New Guinea and the D'Entrecasteaux, Louisiade, Trobriand, and Woodlark archipelagos with localities of included *Toxicocalamus* spp. Inset shows an outline of New Guinea, with focal region represented in the highlighted black border. The map legend specifies species and associated symbols.

delimitation and species tree inference by using an unfixed guide tree under the multispecies coalescent model (A11 option), an advantage in recent versions of BPP (Rannala and Yang, 2003). Results of the A11 option within BPP indicate the probability that a putative species is a separate species (Ruane et al., 2018), allowing more robust species determinations within diverse lineages that have speciated recently. Recent studies have shown that BPP delimits genetic structure within datasets and not specifically species (Sukumaran and Knowles, 2017). Species conceptualization and determination followed the unified species concept (de Queiroz, 2007); thus, species descriptions and final species determinations are based on multiple lines of evidence, including molecular (phylogenies, pairwise comparisons, MSC delimitation) and morphological comparisons.

Results from BPP have been found to be sensitive to settings of its ancestral population size (theta) and divergence time (tau) priors (Leaché and Fujita, 2010; Yang and Rannala, 2010; Ruane et al., 2016, 2018). To avoid this issue, we ran BPP using a variety of different theta and tau prior options (Table 3). Four population size parameters (θs) were used, assigned the inverse-gamma prior IG(3, 0.004), with mean 0.004/(3–1) = 0.002, IG(3, 0.04), with mean 0.02, IG(21, 0.004), with mean 0.0002, and IG(21, 0.04), with mean 0.002. Four divergence times at the root of the species tree (τ0) were assigned the inverse-gamma prior IG(3, 0.002), with mean 0.001, IG(3, 0.02), with mean 0.01, IG(21, 0.002), with mean 0.0001, and IG(21, 0.02), with mean 0.001 (Flouri et al., 2018). Each chosen combination was run three times, confirming convergence of runs on the same number of delimited species. Each run comprised 1,000,000 generations, with a 10% burn-in and a sampling frequency of five. Recent versions (4.0 and newer) of BPP use an inverse gamma distribution for both theta and tau priors instead of the previous gamma distribution of previous versions. An inverse gamma distribution reduces the size of the parameter space, which typically leads to improved mixing of the MCMC.

RESULTS

Toxicocalamus ***goodenoughensis***, sp. nov.

Figures 1–6

Holotype.—LSUMZ 98043 (CCA 15692), an adult female (confirmed by μCT scans), collected by Christopher Austin at low-elevation camp along the banks of the Blawin River among mixture of bush and gardens (−9.2650667, 150.2238833, elevation 147 m), Goodenough Island, Milne Bay Province, Papua New Guinea, on 10 July 2012.

Paratype.—LSUMZ 98042 (CCA 15458), juvenile, Papua New Guinea, Milne Bay Province, Goodenough Island, collected by Christopher Austin crossing bush track near camp along small creek that is a tributary of Moniu River (−9.2899667, 150.21425, elevation 992 m), Goodenough Island, Milne Bay Province, Papua New Guinea, on 20 June 2012.

Diagnosis.—A moderately sized species (holotype 691 total length, 14.1 maximum width) with 15–15–15 dorsal scale rows, 178–186 ventral scales, 37–49 paired subcaudals, preocular scale present and not fused with prefrontal, preocular in contact with prefrontal, internasal, and nasal; prefrontal separated from nasal by contact between preocular and internasal; frontal not fused with supraoculars; internasals not fused; three circumoculars

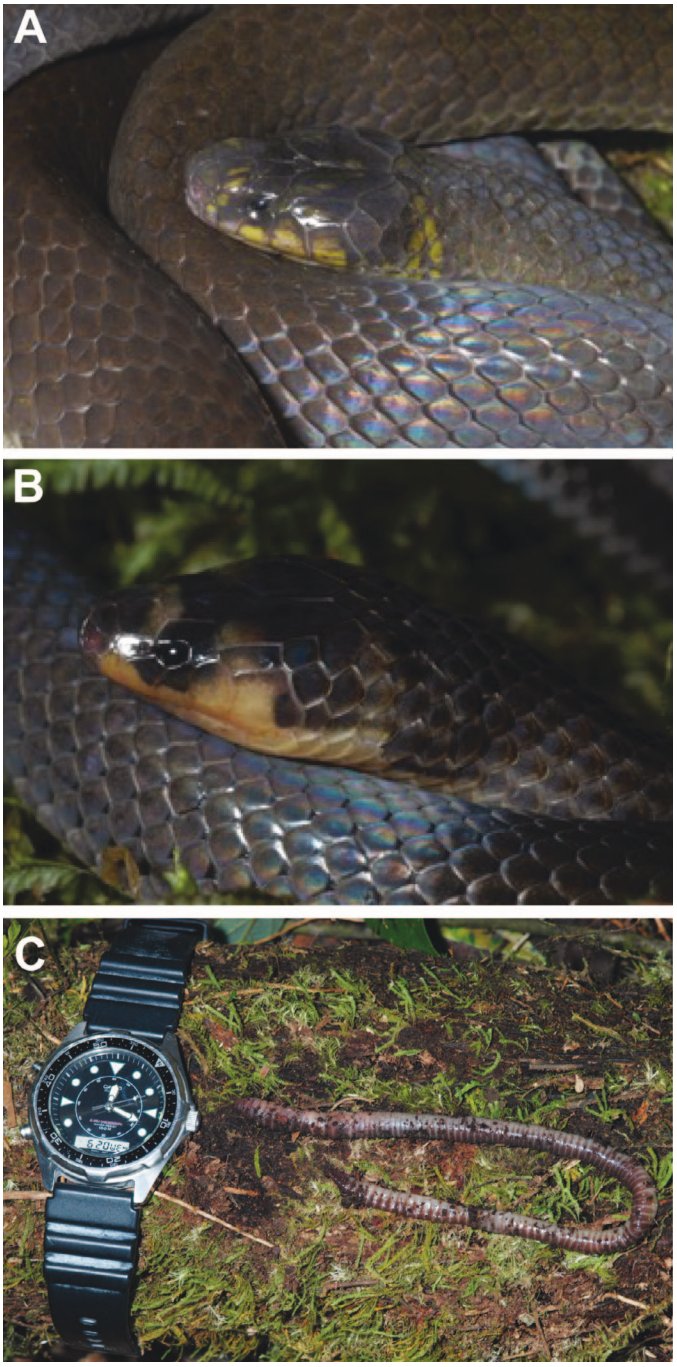

FIG. 2. Photos in life showing (A) *Toxicocalamus goodenoughensis* n. sp., holotype (LSUMZ 98043); (B) *Toxicocalamus goodenoughensis* paratype (LSUMZ 98042); and (C) an earthworm regurgitated by *T. goodenoughensis* (paratype, LSUMZ 98042) after collection, Casio watch case diameter, 44 mm.

(holotype has three on the left and four on the right side [fragmented third supralabial adds a preocular; see description below])—one supraocular, one or two preoculars, one postocular; nasals entire; one anterior temporal, one or two posterior temporals not fused with supralabials; six supralabials, the second in contact with the nasal, preventing contact between nasal and third supralabial; divided cloacal plate; uniform mottling of dark brown on yellowish ventral scales, ventrals progressively become darker brown posteriorly, with ontogenetic lightening of ventrals from dark brown to lighter brown.

TABLE 1. Primers used for loci amplification.

Locus	Forward primer	Reverse primer	Reference(s)
16S	16SF 5′-CGCCTGTTTATCAAAAACAT-3′	16SR 5′-CCGGTCTGAACTCAGATCACGT-3′	Kocher et al., 1989; Metzger et al., 2010
c-mos	G303 5′-ATTATGCCATCMCCTMTTCC-3′	G74 5′-TGAGCATCCAAAGTCTCCAATC-3′	Saint et al., 1998
cytb	L14910 5′-GACCTGTGATMTGAAAAACCAYCGTTGT-3′	H16064 5′-CTTTGGTTTACAAGAACAATGCTTTA-3′	Burbrink et al., 2000; Metzger et al., 2010
RAG-1	G396 5′-TCTGAATGGAAATTCAAGCTGTT-3′	G397 5′-GATGCTGCCTCGGTCGGCCACCTTT-3′	Groth and Barrowclough, 1999; Metzger et al., 2010

TABLE 2. Sequences and individuals included in sequence alignments.

Genus	Species	Catalog no.	*16S*	*c-mos*	*cytb*	*RAG-1*	Latitude	Longitude
Aspidomorphus	*schlegeli*	BPBM 23433	GQ397234	GQ397223	GQ397167	GQ397196	−3.39329	142.528
Aspidomorphus	*schlegeli*	Uncataloged (Metzger et al., 2010)	GQ397238	GQ397228	GQ397169	GQ397200	NA[a]	NA
Aspidomorphus	*muelleri*	ABTC 50600	KF736326	EU366448	AF217814	EU366434	NA	NA
Aspidomorphus	*muelleri*	BPBM 23453	GQ397233	GQ397224	GQ397153	GQ397195	−3.42457	142.519
Aspidomorphus	*lineaticollis*	Uncataloged (Metzger et al., 2010)	GQ397237	GQ397227	GQ397131	GQ397198	NA	NA
Aspidomorphus	*lineaticollis*	Uncataloged (Metzger et al., 2010)	GQ397239	GQ397229	GQ397132	GQ397199	NA	NA
Demansia	*papuensis*	MAGNT-R20514/ ABTC 29355	EU547142	EU546910	EU547044	EU546871	NA	NA
Demansia	*psammophis*	AMS 147748	GQ397240	GQ397230	GQ397172	GQ397201	NA	NA
Demansia	*vestigiata*	SAMA-R34265/ ABTC 11765	EU547143	EU546911	EU547045	EU546872	−12.65	132.88
Toxicocalamus[b]	***loriae* clade 3**	**LSUMZ 93563**	**MT313296**	**MT298113**	**MT298107**	**MT298110**	**−9.339**	**149.1588333**
Toxicocalamus	***goodenoughensis* n. sp.**	**LSUMZ 98042**	**MT313295**	**MT298111**	**MT298105**	**MT298108**	**−9.2899667**	**150.21425**
Toxicocalamus	***goodenoughensis* n. sp.**	**LSUMZ 98043**	**NA**	**MT298112**	**MT298106**	**MT298109**	**−9.2650667**	**150.2238833**
Toxicocalamus	*preussi*	AM 136279	EU547141	EU546909	EU547043	EU546870	−3.3933	142.5283
Toxicocalamus	*loriae* clade 6	BPBM 17987	GQ397235	GQ397225	GQ397170	GQ397197	−10.0145	149.597
Toxicocalamus	*loriae* clade 2	BPBM 41390	KT968664	KU128770	KT778513	KU128742	−7.9538	147.0567
Toxicocalamus	*loriae* clade 2	BPBM 41391	KT968665	KU128771	KT778514	KU128743	−7.9289	147.0458
Toxicocalamus	*holopelturus*	BPBM 20823	KT968666	KU128772	KT778515	KU128744	−11.3345	154.2239
Toxicocalamus	*holopelturus*	BPBM 20824	KT968667	KU128773	KT778516	KU128745	−11.3544	154.2232
Toxicocalamus	*holopelturus*	BPBM 20825	KT968668	KU128774	KT778517	KU128746	−11.3555	154.2246
Toxicocalamus	*holopelturus*	BPBM 20826	KT968669	KU128775	KT778518	KU128747	−11.3366	154.2236
Toxicocalamus	*holopelturus*	BPBM 20827	KT968670	KU128776	KT778519	KU128748	−11.3345	154.2239
Toxicocalamus	*stanleyanus*	BPBM 23455	KT968671	KU128777	KT778520	KU128749	−3.4246	142.5189
Toxicocalamus	*preussi*	BPBM 23456	KT968672	KU128778	KT778521	KU128750	−3.3933	142.5283
Toxicocalamus	*longissimus*	BPBM 39702	KT968673	KU128779	KT778523	KU128751	−9.0844	152.8353
Toxicocalamus	*loriae* clade 3	BPBM 39813	KT968674	KU128780	KT778524	NA	−9.2238	149.1561
Toxicocalamus	*longissimus*	BPBM 42183	KT968675	KU128781	KT778526	KU128752	−9.0378	152.744
Toxicocalamus	*loriae* clade 4	UMMZ 242534	KT968677	NA	KT778528	KU128754	−10.06	151.075
Toxicocalamus	*pachysomus*	BPBM 15771	KT968679	NA	KT778530	KU128756	−10.3471	150.233
Toxicocalamus	*nigrescens*	BPBM 16544	KT968680	NA	KT778531	KU128757	−9.4263	150.8015
Toxicocalamus	*nigrescens*	BPBM 16545	KT968681	NA	KT778532	KU128758	−9.4562	150.5596
Toxicocalamus	*misimae*	BPBM 17231	KT968682	KU128784	KT778533	KU128759	−10.6703	152.7206
Toxicocalamus	*loriae* clade 6	BPBM 17988	KT968683	KU128785	KT778534	KU128760	−10.0145	149.597
Toxicocalamus	*loriae* clade 6	BPBM 17989	KT968684	KU128786	KT778535	KU128761	−10.0171	149.6002
Toxicocalamus	*loriae* clade 6	BPBM 18164	KT968685	KU128787	KT778536	KU128762	−10.0171	149.6002
Toxicocalamus	*loriae* clade 6	BPBM 18166	KT968686	KU128788	KT778537	KU128763	−10.0171	149.6002
Toxicocalamus	*loriae* clade 1	BPBM 19502	KT968687	KU128789	KT778538	KU128764	−9.4439	147.9838
Toxicocalamus	*loriae* clade 1	BPBM 19503	KT968688	KU128790	KT778539	KU128765	−9.4447	148.0092
Toxicocalamus	*loriae* clade 1	BPBM 19504	KT968689	KU128791	KT778540	KU128766	−9.4447	148.0092
Toxicocalamus	*loriae* clade 1	BPBM 19505	KT968690	KU128792	KT778541	KU128767	−9.4439	147.9838
Toxicocalamus	*loriae* clade 1	BPBM 19506	KT968691	KU128793	KT778542	KU128768	−9.4439	147.9838
Toxicocalamus	*mintoni*	BPBM 20822	KT968692	NA	KT778543	KU128769	−11.4961	153.4241

[a] NA = not applicable.
[b] Bold entries indicate new sequences generated for this study that are now deposited on GenBank.

Toxicocalamus goodenoughensis can be distinguished from *T. holopelturus* by having paired subcaudals (vs. single); from *T. mintoni*, *T. stanleyanus*, *T. cratermontanus*, *T. misimae*, *T. longissimus*, *T. pumehanae*, *T. buergersi*, and *T. preussi* by having a preocular scale unfused to the prefrontal scale (vs. fused in listed congeners); and from *T. nigrescens*, *T. loriae*, *T. spilolepidotus*, *T. grandis*, and *T. ernstmayri* by having internasal scales contacting preocular scales, preventing contact between nasals and prefrontals (vs. internasals and preoculars separated by contact between nasals and prefrontal scales).

Toxicocalamus goodenoughensis is most similar morphologically to *T. pachysomus* but differs by having undivided (or entire) nasal scales completely surrounding the nares; pale yellow on supralabials (vs. purple blotches); yellow nape band present (vs. nape unbanded); more than 175 ventral scales (vs. 171 ventral scales); dark gray-brown dorsum (vs. medium brown); and dark brown mottling on yellow ventral scales, darkening toward cloaca (vs. uniform light brown).

Description of Holotype.—Adult female. Rostral broader (4.0) than tall (2.4); internasals triangular, wider (3.2) than long (1.8); prefrontals unfused to preoculars (Figs. 3C, 4), right slightly longer (3.9) than wide (3.2) and left wider (3.2) than long (3.1), bordered below by preoculars and internasals; preoculars not bilaterally symmetrical, with two on the right side and one on the left (smaller of two on right side appears to be result of fragmented third supralabial; see additional comments in Remarks and Figs. 3C, 4A), primary preocular rectangular with rounded anterior and posterior margins, not fused with supraoculars; parietal scales more than twice as long (right 8.1, left 8.2) than wide (each 3.3). Nasals undivided, surrounding entirety of nares; postocular single, round, larger than eye (diameter 1.6); anterior temporal single, rectangular, positioned above fifth and six supralabials; posterior temporals two, dorsal posterior

FIG. 3. *Toxicocalamus goodenoughensis* n. sp., showing the (A) dorsum of *T. goodenoughensis* holotype (LSUMZ 98043), (B) venter of holotype, (C) right view of head of holotype, (D) dorsum of *T. goodenoughensis* paratype (LSUMZ 98042), (E) venter of paratype, and (F) right view of head of paratype. Scale bars aside dorsum and venter images (A), (B) and (D), (E) are each 2 cm. Scale bars aside head images (C) and (F) are each 5 mm.

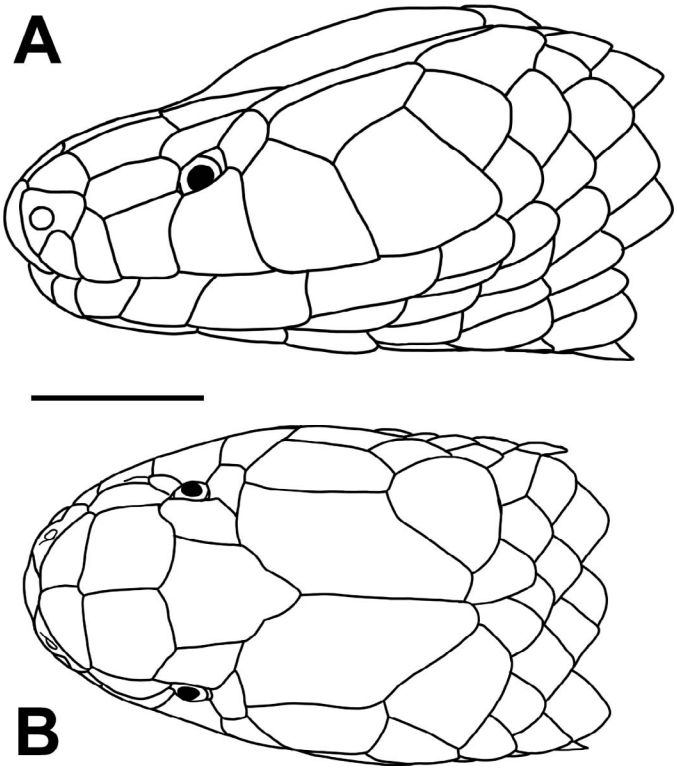

FIG. 4. Line drawings highlighting head scalation of the holotype. Left (A) and (B) dorsal view of the *T. goodenoughensis* holotype (LSUMZ 98043). The scale bar for (A) and (B) is 6 mm.

TABLE 3. BPP priors and posterior probabilities for multispecies coalescent-based species delimitation.

Run no.	Theta shape	Theta parameter	Tau shape	Tau parameter	No. of species delimited	Posterior probability
1	3	0.004	3	0.002	14	0.999932
2					14	0.999916
3					14	0.999910
1	3	0.004	3	0.02	14	0.999912
2					14	0.999921
3					14	0.999920
1	3	0.04	3	0.002	14	0.896352
2					14	0.896636
3					14	0.895612
1	3	0.04	3	0.02	14	0.896093
2					14	0.895232
3					14	0.895203
1	21	0.004	21	0.002	14	0.999937
2					14	0.999934
3					14	0.999941
1	21	0.004	21	0.02	14	0.999999
2					14	0.999999
3					14	1.0000
1	21	0.04	21	0.002	14	0.999775
2					14	0.999760
3					14	0.999772
1	21	0.04	21	0.02	14	0.999838
2					14	0.999852
3					14	0.999864

temporal larger than more ventral, positioned above the sixth supralabial and separating it from the parietals. Supralabials six, third and fourth touching eye (except only fourth on right eye; see Remarks); infralabials six, first four in contact with anterior genials (anterior and posterior). Mental triangular, wider (3.0) than tall (1.6); anterior genials touching, separated anteriorly by both first infralabials touching; posterior genials touching; gular scale between posterior genials, 2.5 long by 2.0 wide. Eye small (diameter 1.3); pupil round.

Dorsal scale rows 15–15–15, smooth without apical pits. Ventrals 186, 3.5 times wider than long; cloacal scale divided; subcaudals 37. Tail with conical spine (length 4).

Measurements of the Holotype.—Total length = 691, SVL = 602, tail length = 89, eye–naris distance = 4.2, internarial distance = 3.3, head length (rostral to posterior margin of parietals) = 16.3, head width (widest point anterior to quadrate) = 11.1.

Dentition of the Holotype.—Maxilla with seven teeth (II, five); dentary with 11 teeth; palatine with 11 (right) and 10 (left) teeth; pterygoid with teeth extending posteriorly to level of the basisphenoid and basioccipital suture, teeth decreasing in size posteriorly.

Counts and Measurements of the Paratype.—Dorsal scale rows 15–15–15. Ventrals 178; subcaudals 49. Total length = 321, SVL = 271, tail length = 50, eye–naris distance = 2.4, internarial distance = 1.6, eye width = 1, head length = 9.5, head width = 6.5.

Dentition of the Paratype.—Maxilla with 7 teeth (II, five); dentary with 11 teeth; palatine with 12 teeth; pterygoid with teeth extending posteriorly to level of the basisphenoid and basioccipital suture, teeth decreasing in size posteriorly.

Morphological Variation.—Regarding scalation, the only important difference between the holotype and paratype is with the preoculars. In the holotype, as mentioned above, there are two preoculars on the right side, with only one on the left side. In the paratype, both sides have a single preocular. Because of the asymmetry in the holotype, symmetry in the paratype, and the "X" shaped markings on the third supralabial directly underneath the preocular in question (Fig. 3C), we think that this second preocular could be because of fragmentation of the third supralabial, perhaps from an injury. The left side has been illustrated (Fig. 4A) to show an unfragmented preocular.

Genetic Variation.—Phylogenetic analyses indicate that *T. goodenoughensis* is most closely related to *T. nigrescens* from Fergusson Island (Figs. 1, 6). Of the four loci, *T. goodenoughensis* is most divergent from *T. nigrescens* in *cytb*, with 5.67% sequence divergence. The *T. goodenoughensis* + *T. nigrescens* clade is sister to a *T. loriae* clade 4 + *T. pachysomus* clade, with *T. goodenoughensis* having 6.65 and 7.15% *cytb* sequence divergence to these species, respectively.

Color in Life.—The holotype (Fig. 2A) has a universally colored dorsum that is a dark gray-brown with light iridescence. All dorsal patterning is found on the nape and face but is faint and mottled. On the nape, immediately after the temporal scales, pale mottled yellow coloring extends toward dorsum from venter on both sides, but it does not connect into a complete band, leaving the space immediately posterior from parietals the dark gray brown seen on rest of dorsum. On the face, the pale yellow seen on the venter and chin scales extends up onto the supralabials about halfway. Again, the color is not uniform, with some mottling. Lastly, the pale yellow extends from the chin anterior to the eye and onto the preocular and prefrontal scales, almost connecting and forming a snout band at the prefrontal suture. The ventrals are pale yellow with dark brown mottling that increases posteriorly toward the cloaca, making the last ventral scale the darkest. The subcaudal scales are uniform dark brown and darker than all ventral scales.

The paratype (Fig. 2B) exhibits the same overall patterning of the holotype, but the contrast between the dark gray-brown dorsum and pale yellow venter is stronger. The nape band again

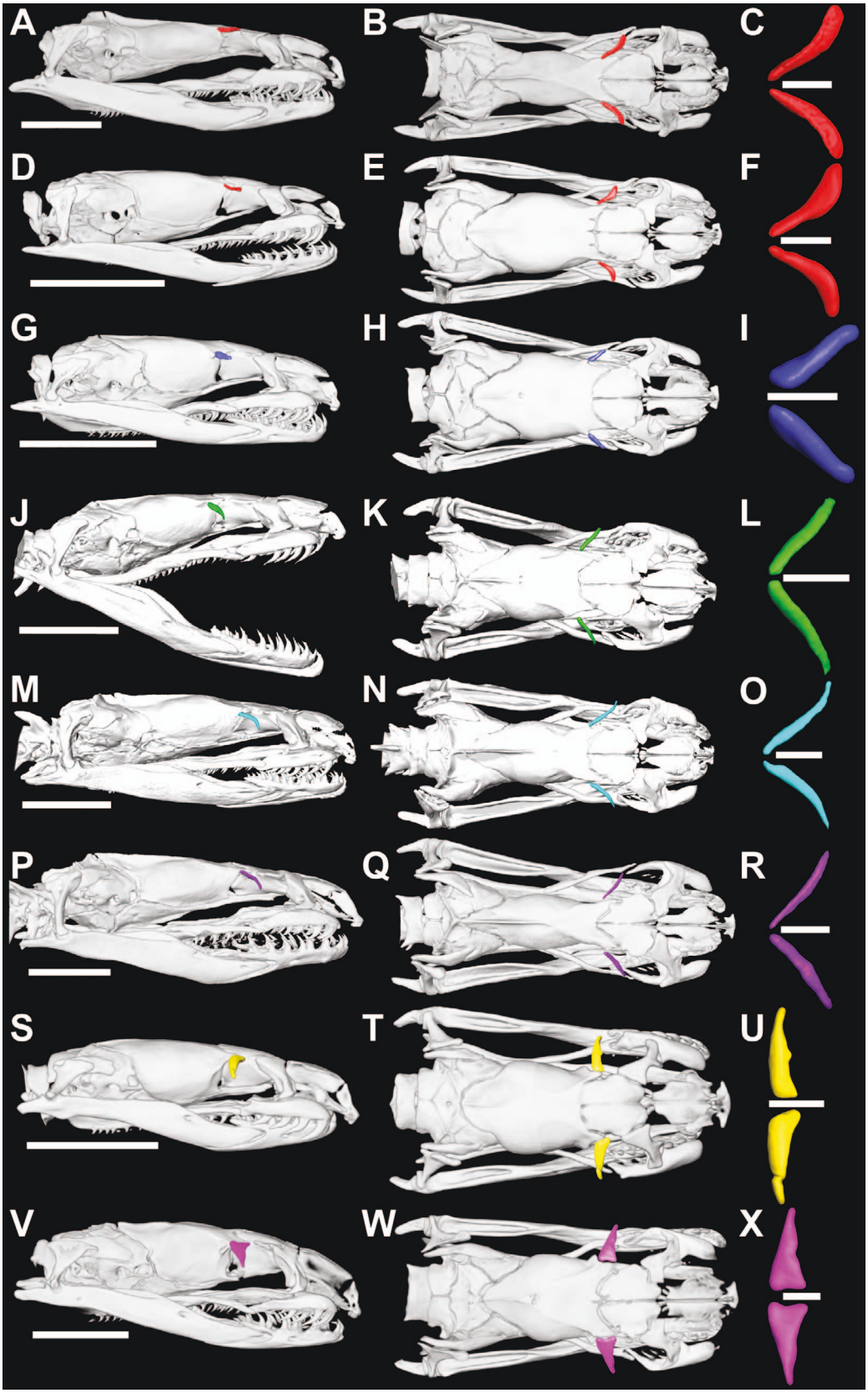

FIG. 5. μCT scans of the new species, highlighting postfrontal bone variation compared with selected congeners. Each species is represented by a right and dorsal view and then a close up of the postfrontal bones. Postfrontal bones were photographed in direction and orientation that they are attached to the skull to highlight the difference in angles. All skull scale bars are 5 mm. All postfrontal bone scale bars are 1 mm, except that of (F), which is 0.5 mm. (A–C) Holotype (LSUMZ 98043) of *T. goodenoughensis* n. sp. (D–F) Paratype (LSUMZ 98042) of *T. goodenoughensis*. (G–I) A voucher (LSUMZ 93563) of *T. loriae* clade 3. (J–L) Holotype (BPBM 20822) of *T. mintoni*. (M–O) Holotype (BPBM 16545) of *T. nigrescens*. (P–R) Holotype (BPBM 15771) of *T. pachysomus*. (S–U) Holotype (AMNH 76660) of *T. holopelturus*. (V–X) Holotype (AMNH 85745) of *T. spilolepidotus*.

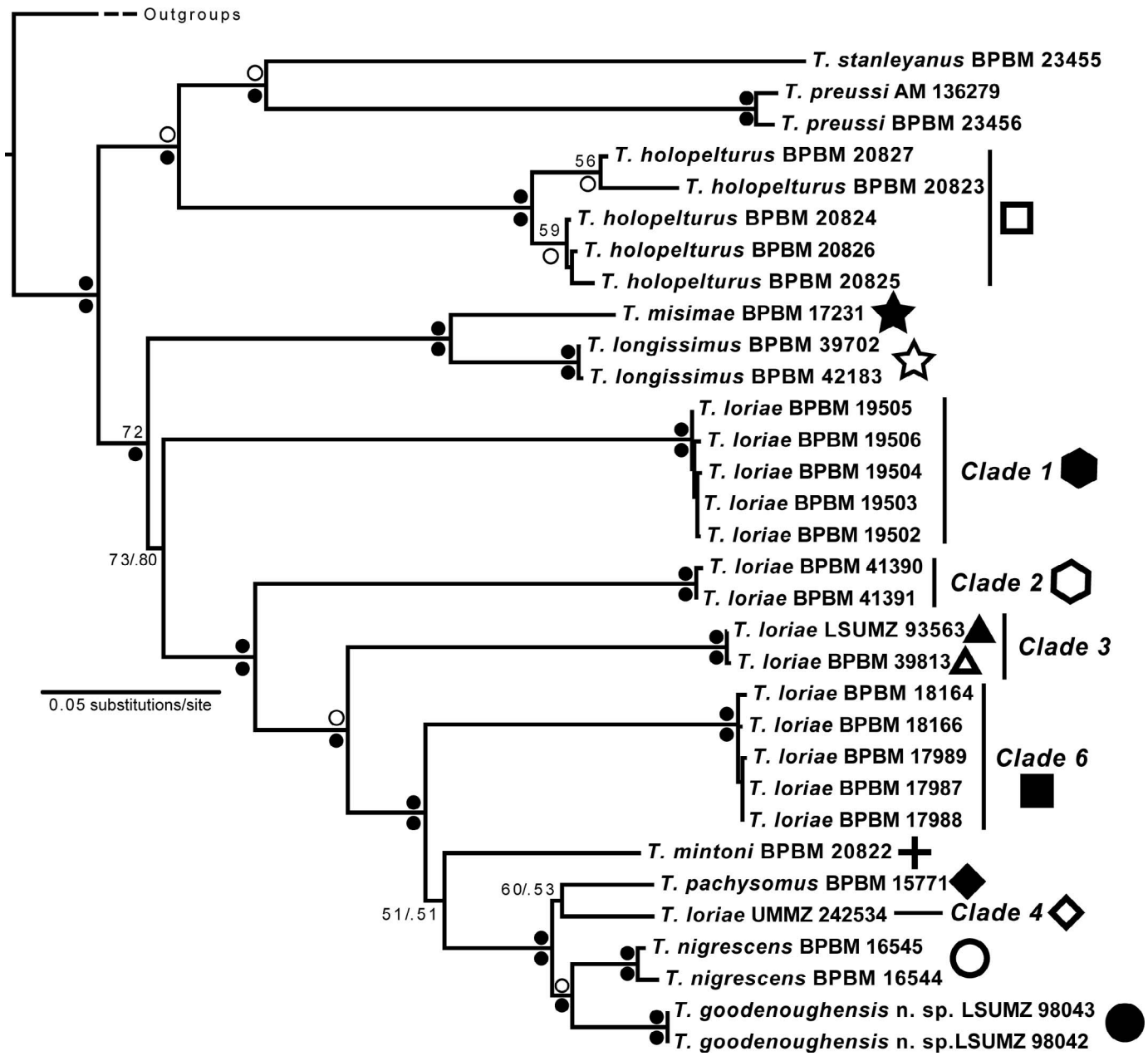

FIG. 6. *Toxicocalamus* spp. phylogeny representing 11 of the 16 proposed species, based on the concatenated sequence alignment. Also included are undescribed clades of cryptic diversity identified as *T. loriae* (see Strickland et al., 2016). Phylogeny was inferred using RAxML. Circles above branches correspond to bootstrap support values: black meaning ≥95 and white meaning 75–94. Circles below branches correspond to posterior probabilities produced by MrBayes: black meaning ≥0.95 and white meaning 0.85–0.94. Bootstrap support or posterior probabilities below 75 or 0.85, respectively, have been indicated. Symbols aside species relates to localities on Figure 1. There was 100% concordance between RAxML and MrBayes trees of the concatenated dataset.

almost completes behind the parietal scales, but does not. A pale yellow band at the frontal-prefrontal suture is present, but it does not connect with the pale yellow extending toward the dorsum from the ventral side of chin on supralabials two and three. The pale color from the venter extends further up the dorsum at supralabial five and six, extending toward dorsum all the way to the anterior margin of the parietal scales but stopping short of the frontal scale. The ventral scales again become darker toward the cloaca, but they are darker than the ventrals of the holotype.

Color in Preservative.—The color in preservative of both type specimens is the same as the color patterns in life. Both specimens still remain iridescent.

Etymology.—The specific epithet, *goodenoughensis*, refers to Goodenough Island, where both specimens were found. Goodenough is the northernmost island in the D'Entrecasteaux Archipelago (Fig. 1).

Distribution.—These are the only two specimens known of this species and the first representatives of *Toxicocalamus* collected from Goodenough Island. For now, the species can be considered endemic to the island because no other representatives of this species have been found.

Ecological Notes.—As with many species in this genus, ecological observations are limited for this species. Austin observed that the paratype regurgitated an earthworm while in a collecting bag (Fig. 2C). This observation coincides with

previous reports of *Toxicocalamus* species feeding on earthworms (O'Shea, 1996; Shine and Keogh, 1996; O'Shea et al., 2015).

Deposited Material.—μCT scans of holotype and paratype comprise scans of the bodies and heads deposited on Morphosource (S45879 for holotype scans, S45878 for paratype). See Table 2 for GenBank accessions information.

Remarks.—Despite being most similar scalationally to *T. pachysomus*, phylogenetic analysis demonstrates that *T. goodenoughensis* is most closely related to *T. nigrescens* from Fergusson Island, the middle island in the three-island D'Entrecasteaux Archipelago (Figs. 1, 6). Together, *T. goodenoughensis* + *T. nigrescens* are sister to a clade comprising a mainland + Normanby Island (D'Entrecasteaux) clade, *T. pachysomus* + *T. loriae* clade 4.

Species Delimitation.—All BPP runs, independent of theta and tau prior settings, found strong evidence (>0.95 posterior probability) for the delimitation of *T. goodenoughensis* as a distinct species. Regarding delimitation of all species included, all used combinations of parameters delimited 14 species with strong support (>0.99 poster probability) except for two combinations, theta-IG(3, 0.04) and tau-IG(3, 0.002) and theta-IG(3, 0.04) and tau-IG(3, 0.02), which returned posterior probabilities ~0.90. In each of these delimitations, the alternative delimitation to all 14 species being distinct was the collapsing of *T. loriae* clade 4 and *T. pachysomus* as one species (~0.10 posterior probability) (Table 3). Looking at the phylogeny (Fig. 6), this relationship has the weakest support of any terminal clades and *cytb* sequence divergence 6.14% between these species. The common parameter setting between these two combinations was the theta parameter, i.e., ancestral population size, as IG(3, 0.04). Because of all other parameter settings delimiting with high posterior probability the presence of 14 species in our dataset, the low (~0.10) probability of the collapsed species, and the fact that *T. pachysomus* and *T. loriae* clade 4 are both morphologically diagnosable and geographically isolated (Fig. 1), we do not identify these species as one.

μCT Scans.—μCT scans reveal similarities in postfrontal bone shape between the holotype and paratype of this species (Fig. 5A–F). Postfrontal bones in both individuals are curved, or sickle-shaped, and directed forward toward the snout. Maxillary dentition was identical between the holotype and paratype. Cranial differences observed in μCT scans include the width of the parietal bone (holotype parietal width/length = 3.5/7.4 [47.3%], paratype = 2.9/4.9 [59.2%]) and the depth of the sagittal crest (holotype crest depth/parietal depth = 0.76/4.6 [16.5%], paratype = 0.23/2.9 [7.9%]), differences that have been shown to be related to ontogenetic changes in snakes (holotype SVL = 602, paratype SVL = 271) (Rossman, 1980).

Discussion

Toxicocalamus goodenoughensis of Goodenough Island comprises the second described species of the genus endemic to the D'Entrecasteaux Archipelago (Fig. 1). The middle island of the Archipelago, Fergusson Island, hosts the endemic *T. nigrescens* described in 2017 (Kraus, 2017b) (Fig. 1). The third, and southern-most island of the D'Entrecasteaux Archipelago, Normanby Island, hosts a species morphologically indistinguishable from *T. nigrescens* (see Kraus, 2017b) but genetically unique and is included in the analyses herein as *T. loriae* clade 4 (Fig. 6; also see Strickland et al., 2016). Both *Toxicocalamus* and another terrestrial hydrophiine, *Aspidomorphus*, exhibit this unique pattern of one endemic lineage per island within the D'Entrecasteaux Archipelago. Metzger et al. (2010) showed within *Aspidomorphus* the presence of many cryptic lineages that are likely undescribed species, including splits between *Aspidomorphus* cf. *lineaticollis* specimens found on each island within the D'Entrecasteaux Archipelago. *Toxicocalamus* and *Aspidomorphus* are closely related and comprise the only terrestrial hydrophiines found within the D'Entrecasteaux Archipelago. The islands within the D'Entrecasteaux Archipelago host a diversity of non-elapid snakes as well, including boids (*Candoia*), colubrids (*Boiga*, *Dendrelaphis*, *Stegonotus*, *Tropidonophis*), pythonids (*Apodura*, *Morelia*), and gerrhopilid and typhlopid blindsnakes (O'Shea, 1996; Kraus, 2017a). However, non-elapid genera found within the archipelago are usually represented by one species found archipelago-wide (O'Shea, 1996). Perhaps this is because of reduced vagilities or speciation histories of the semifossorial hydrophiines compared with other herpetofauna, but it may likely be because of the need to revisit population level biogeography and systematics of all New Guinea reptiles and amphibians found among the offshore islands of New Guinea.

To date, there are 16 accepted species (including *T. goodenoughensis*) that are found as far east as Rossel Island within the Louisiade Archipelago (Fig. 1) and as far west as the Fakfak Peninsula south of the Bird's Head in Indonesian Papua, with no records of the genus from the Southern Trans-Fly region (see fig. 1 of O'Shea et al., 2018). Currently, the epicenter of diversity appears to be the eastern New Guinea peninsula and associated archipelagos, with four species reported from the mainland and six species (including *T. goodenoughensis*) reported from nearby archipelagos (O'Shea et al., 2018). The complex tectonic history of the eastern New Guinea and its peripheral archipelagos further complicates the evolutionary history of *Toxicocalamus*. Before the formation of the Woodlark Rift, the modern-day Woodlark (northern boundary of Woodlark Basin) and Pocklington (southern boundary) rises were once a contiguous extension of a much larger ancestral and subaerial eastern Papuan Peninsula. Beginning ~6 mya, Woodlark rifting split the Papuan Peninsula, created the Woodlark Basin, and commenced the sinking of the Woodlark and Pocklington rises because of crustal extension (Taylor et al., 1995, 1999; van Ufford and Cloos, 2005; Baldwin et al., 2012). It is thus possible that modern-day island endemics on the Louisiade and Woodlark archipelagos are products of vicariant allopatric speciation via rising sea levels and Woodlark Rift formation and resulting tectonic plate movement. Therefore, combined increases in sea level and rise sinking are thought to have created the modern-day Louisiade, Trobriand, and Woodlark archipelagos, invoking the more probable scenario that these snakes are products of vicariant allopatry after island formation and not over-water dispersal from the mainland. By contrast, the modern-day D'Entrecasteaux Archipelago is the result of significant uplift above sea level ~3 mya (after the onset of Woodlark rifting) because of the presence of metamorphic core complexes within the island chain (Little et al., 2011; Baldwin et al., 2012). In addition, during glacial maxima, it is quite possible that the three D'Entrecasteaux islands were reconnected to the mainland (Mayr and Diamond, 2001; Lavery et al., 2016). Regarding D'Entrecasteaux-endemic *Toxicocalamus* species, two biogeographic hypotheses seem likely: 1) metamorphic core complex uplift created these islands from previously submerged landmasses, allowing dispersal of *Toxicocalamus* to these islands during glacial maxima; or 2) metamorphic core complex uplift of previously subaerial landmasses allopatrically separated the

most recent common ancestor (MRCA) of these taxa in similar manner and timing as the Louisiade, Trobriand, and Woodlark archipelagos. At this time, without a dated phylogeny and rigorous biogeographic reconstructions, we cannot differentiate between these two hypotheses.

Phylogenetic analyses used a dataset comprising of mostly sequences generated from a well-executed phylogenetic assessment of *Toxicocalamus* by Strickland et al. (2016). The primary objective for our study was to describe the new species and to generate a hypothesis of phylogenetic relatedness of the new species to their congeners; however, our resulting phylogeny possesses some topological discrepancies compared with the tree of Strickland et al. (2016; see fig. 3). The primary difference between our phylogeny (Fig. 6) and their phylogeny relates to the position of *T. holopelturus*, a species endemic to Rossel Island of the Louisiade Archipelago (Fig. 1). Our phylogeny finds, with strong support, *T. holopelturus* sister to the *T. stanleyanus* + *T. preussi* clade, both mainland New Guinea endemics, and the westward-most–included samples in our dataset. Strickland et al. (2016) finds *T. holopelturus* sister to all other congeners except the *T. stanleyanus* + *T. preussi* clade, also with strong support. An additional discrepancy includes the placement of the *T. misimae* + *T. longissimus* clade. Our analysis finds this clade sister to a clade comprising all other congeners but *T. holopelturus* + (*T. stanleyanus* + *T. preussi*). Strickland et al. (2016) found the *T. misimae* + *T. longissimus* clade to be sister to *T. loriae* clade 1 ("true" *T. loriae* [see Kraus, 2017b]), where we did not find this sister relationship. Other than the differences described above, topologies between our tree and that of Strickland et al. (2016) were identical. All discrepancies in topology between our tree and that of Strickland et al. (2016) occur at early branching points. The trees also differ in the datasets that generated them. Our dataset comprised four Sanger-sequenced loci, compared with seven of Strickland et al. (2016). However, despite fewer loci, our tree has comparable or stronger support values at the nodes in question.

Small multilocus datasets for groups that have rapidly diversified within short time frames such as *Toxicocalamus* can be susceptible to incomplete lineage sorting. For this reason, we used BPP, a coalescent-based species delimitation method, to provide an additional line of evidence for the new species described herein. In addition to all species being monophyletic in phylogenetic analyses, BPP analyses provided strong support that the 14 taxa included in the dataset (9 accepted, 5 cryptic and undescribed) appear to be unique evolutionary units and not because of incomplete lineage sorting. Because BPP has been demonstrated to delimit genetic structure and not species (Sukumaran and Knowles, 2017), we accept these delimited taxa as species and not populations because in addition to the BPP results, the delimited taxa can be diagnosed morphologically as well, adhering to the unified species concept (de Quieroz, 2007), thus taking multiple lines of evidence into decision-making before final species determination.

Using μCT scanning, we identify species-specific variation in postfrontal bone shape within *Toxicocalamus* (Fig. 5). Although μCT scans elucidated novel interspecific differences, McDowell (1969) first identified postfrontal (described as postorbital in his work; Palci and Caldwell, 2013; Garberoglio et al., 2019) presence–absence variation that led him to separate some species into separate subgenera: *Apistocalamus* Boulenger, 1898 (postfrontal present); *Toxicocalamus* Boulenger, 1896 (absent); and *Ultrocalamus* Sternfeld, 1913 (absent). According to McDowell (1969), species lacking postfrontal bones comprise *T. longissimus*, *T. misimae*, *T. stanleyanus*, *T. preussi*, and *T. buergersi*, leaving *T. holopelturus*, *T. grandis*, *T. loriae*, and *T. spilolepidotus* with postfrontal bones. Species descriptions since McDowell (1969) have not addressed the presence or absence of the postfrontal bone; however, a preliminary, and growing, dataset of genus-wide μCT scanning aimed at revising the genus morphologically and with next-generation sequencing (Roberts and Austin, unpubl. data) has confirmed the presence of postfrontal bones in the holotypes of *T. holopelturus*, *T. mintoni*, *T. nigrescens*, *T. pachysomus*, and *T. spilolepidotus*; a voucher identified as *T. loriae* clade 3; and the new species described herein. We have also confirmed the absence of a postfrontal bone in the *T. misimae* holotype.

Based on the dataset presented herein (Fig. 5), it appears that postfrontal bone morphology can be placed into three categories within *Toxicocalamus*: directed forward (Figs 5A–R; five species), directed lateral or perpendicular to cranium (Figs 5S–X; two species), and absent (*T. misimae*). Based on the work from Strickland et al. (2016) and the phylogeny produced herein (Fig. 6), the subgenera proposed by McDowell are paraphyletic. Of the nine species included in our μCT dataset, all but one, *T. spilolepidotus*, are represented in our phylogeny. *Toxicocalamus spilolepidotus* is known only from its type material, and no ethanol-preserved tissue exists.

Of the five species McDowell reported with absent postfrontals, four are represented in our phylogenetic analysis (*T. longissimus*, *T. misimae*, *T. preussi*, *T. stanleyanus*), and these four species are represented by two strongly supported sister pairs (*T. preussi* + *T. stanleyanus*, *T. longissimus* + *T. misimae*). We have not scanned representatives of *T. loriae* clade 1, clade 2, clade 4, and clade 6, but if we assume these species do have postfrontal bones because of their morphological affinity to *T. loriae*, it is unclear whether the common ancestor to all *Toxicocalamus* had postfrontal bones or not. Both scenarios are equally parsimonious in our analyses, with two independent losses assuming postfrontals in the MRCA or two independent acquisitions of postfrontals with a bone-less MRCA. The same is true if we assign postfrontal bone presence–absence on to Strickland's phylogeny, with one acquisition and one subsequent loss (still two steps) with the bone-less MRCA scenario. However, in accordance with Dollo's law (Dollo, 1893; Gould, 1970), we are inclined to think that the MRCA most likely had postfrontals and that subsequent losses have resulted in extant congeners lacking these features. Other elapid groups have lost the postfrontal bone, i.e., Asian coral snakes (*Sinomicrurus*) and New World coral snakes—*Micruroides* and *Micrurus* (Slowinski et al., 2001). However, in these other genera, postfrontal absence is synapomorphic. *Toxicocalamus* may be the only known genus with intrageneric variation in postfrontal presence and absence and postfrontal shape (between species that have the bone).

Sampling deficiencies from across the island could likely be obscuring our understanding of true species diversity and genetic structure within wide-ranging species of *Toxicocalamus*. Future field collections along the southern coast and northwestern regions of Papua New Guinea are critical for improving our hypotheses regarding evolutionary relatedness and phylogeography of *Toxicocalamus*. In the meantime, the next actions for better assessing phylogeography lie in next-generation sequencing (NGS). The applications of NGS to diverse groups with cryptic taxa facilitate systematics through amount of data, with thousands of loci compared with a handful of Sanger-sequenced loci, and through access to new methods that are optimized for large-scale NGS datasets. Thousands of loci

compared with several will provide more robust hypothesis testing of phylogenetic relationships. Importantly, recent protocols have had success using formalin-fixed intractable tissues (Ruane and Austin, 2017; McGuire et al., 2018), permitting the inclusion of species known from just their type material or other intractable specimens, i.e., *T. buergersi*, *T. cratermontanus*, *T. ernstmayri*, *T. grandis*, *T. pumehanae*, and *T. spilolepidotus*.

Dichotomous Key to *Toxicocalamus**

1a) Subcaudals entire ..... *T. holopelturus*
1b) Subcaudals divided 2
2a) Preocular unfused to prefrontal 3
2b) Preocular fused to prefrontal 9
3a) Internasal and preocular in contact, separating nasal from prefrontal 4
3b) Internasal and preocular not in contact, separated by contact of nasal with prefrontal 5
4a) Nasal scales clearly divided by large nares; purple markings on supralabials; nape uniform and unbanded; medium brown dorsum; ventrals <175, light brown ..... *T. pachysomus*
4b) Nasal scales entire, surrounding nares; pale yellow markings on supralabials; yellow nape band; dark gray-brown dorsum; ventrals >175, with dark brown mottling on yellow, darkening toward cloaca ..... ***T. goodenoughensis* n. sp.**
5a) Dorsum uniform dark gray, without pale spots ... 6
5b) Dorsum dark grey or brown with pale spots or markings 7
6a) Ventrum banded with dark gray; subcaudals uniformly gray ..... *T. nigrescens*
6b) Ventrum immaculately yellow; subcaudals yellow with gray margins ..... *T. loriae*
7a) Almost all dorsal scales except vertebral row with distinct pale yellow spot; ventrals with broad black spot on each ..... *T. spilolepidotus*
7b) Posterior half of dorsal scales pale, lacking distinct pale spot in scale 8
8a) Postocular single, not paired ..... *T. grandis*
8b) Postocular paired, not single ..... *T. ernstmayri*
9a) Frontal fused to supraoculars ..... *T. mintoni*
9b) Frontal unfused to supraoculars 10
10a) Prefrontal unfused with internasal 11
10b) Prefrontal fused with internasal 14
11a) Cloacal scale entire; 5 supralabials; venter without dark stripes 12
11b) Cloacal scale divided; 6 (rarely 7) supralabials; venter with a pair of longitudinal dark stripes .. 13
12a) Ventral scales <260; last supralabial taller than broad; ventrals and subcaudals immaculate white or white with small, lateral brown spots; pale nuchal collar present ..... *T. stanleyanus*
12b) Ventral scales >260; last supralabial broader than tall; ventrals and subcaudals brown, barred with dark brown anteriorly and posteriorly; pale nuchal collar absent ... *T. cratermontanus*
13a) 15 dorsal scale rows at midbody ..... *T. mismae*
13b) 17 dorsal scale rows at midbody ... *T. longissimus*
14a) Temporal scale unfused with supralabial, separating last supralabial from parietal .. *T. pumehanae*
14b) Temporal scale fused with supralabial, last supralabial contacting parietal 15
15a) Four supralabials; postocular fused with supraocular; 15 dorsal scale rows at midbody ..... *T. buergersi*
15b) Five supralabials; postocular usually distinct from supraocular; usually 13 (rarely alternating between 13 and 15) dorsal scale rows at midbody ..... *T. preussi*

*Based on Kraus (2009) and modified with updated morphological data from Kraus (2017b), O'Shea et al. (2015, 2018), and the new species described in this paper.

Acknowledgments.—For his invaluable discussions and guidance on the description, *Toxicocalamus* ecology, and New Guinea geological history, we thank Fred Kraus (University of Michigan Museum of Zoology). We also thank the two anonymous reviewers who provided thorough and considerate reviews that greatly improved the quality of this manuscript. For help with specimen loans, we thank Seth Parker (LSUMZ), José Rosado (Museum of Comparative Zoology, Harvard University), Frank Burbrink and David Kizirian (American Museum of Natural History), and Molly Hagemann (Bernice P. Bishop Museum). For help with field collections, we thank Bulisa Iova (Papua New Guinea National Museum and Art Gallery). For generating sequence data, we thank Catherine Newman (University of Louisiana Monroe). Lastly, for assistance with μCT scanning and analyses, we thank Dave Blackburn, Coleman Sheehy, Ed Stanley, and Daniel Paluh at the Florida Museum of Natural History and Justin Gladman and Mark Walters at the Shared Materials Instrumentation Facility at Duke University. All handling of animals and biosecurity were performed within the guidelines of the Louisiana State University Institutional Animal Care and Use Committee (ID 11-094). This research was funded by National Science Foundation grants DEB 1146033 and DEB 1926783 to CCA.

Literature Cited

Allison, A. 1996. Zoogeography of amphibians and reptiles of New Guinea. Pp. 407–436 in A. Keast and S. E. Miller (eds.), The Origin and Evolution of Pacific Island Biotas, New Guinea to Eastern Polynesia: Patterns and Processes. SPB Academic Publishing, The Netherlands.

Austin, C. C., M. Spataro, S. Peterson, J. Jordan, and J. D. McVay. 2010. Conservation genetics of Boelen's python (*Morelia boeleni*) from New Guinea: reduced genetic diversity and divergence of captive and wild animals. Conservation Genetics 11:889–896.

Baldwin, S. L., P. G. Fitzgerald, and L. E. Webb. 2012. Tectonics of the new Guinea region. Annual Review of Earth and Planetary Sciences 40:495–520.

Bogert, C. M., and B. L. Matalas. 1945. Results of the Archbold Expeditions. No. 53: a review of the elapid genus *Ultrocalamus* of New Guinea. American Museum Novitates 1284:1–8.

Boulenger, G. A. 1896. Description of a new genus of elapine snakes from Woodlark Island, British New Guinea. Annals and Magazine of Natural History 18:152.

———. 1898. An account of the reptiles and batrachians collected by Dr. L. Loriae in British New Guinea. Annali Del Museo Civico Di Storia Naturale Di Genova 38:694–720.

———. 1903. Descriptions of new reptiles from British New Guinea. Proceedings of the Zoological Society of London 2:125–129.

———. 1914. An annotated list of the batrachians and reptiles collected by the British Ornithologists Union Expedition and the Wollaston Expedition in Dutch New Guinea. Transactions of the Zoological Society of London 20:247–274.

Burbrink, F. T., R. Lawson, and J. B. Slowinski. 2000. Mitochondrial DNA phylogeography of the polytypic North American rat snake (*Elaphe obsoleta*): a critique of the subspecies concept. Evolution 54:2107–2118.

Calvete, J. J., P. Ghezellou, O. Paiva, T. Matainaho, A. Ghassempour, H. Goudarzi, F. Kraus, L. Sanz, and D. J. Williams. 2012. Snake venomics of two poorly known Hydrophiinae: comparative proteomics of the venoms of terrestrial *Toxicocalamus longissimus* and marine *Hydrophis cyanocinctus*. Joural of Proteomics 75:4091–4101.

de Queiroz, K. 2007. Species concepts and species delimitation. Systematic Biology 56:879–886.

Dollo, L. 1893. Les Lois de l'evolution. Bulletin de la Société Belge de Géologie 7:164–166.

Dowling, H. G. 1951. A proposed standard system of counting ventrals in snakes. British Journal of Herpetology 1:97–99.

Edgar, R. C. 2004. MUSCLE: multiple sequence alignment with high accuracy and high throughput. Nucleic Acids Research 32:1792–1797.

Flouri, T., X. Jiao, B. Rannala, and Z. Yang. 2018. Species tree inference with BPP using genomic sequences and the multispecies coalescent. Molecular Biology and Evolution 35:2585–2593.

Garberoglio, F. F., S. Apesteguía, T. R. Simões, A. Palci, R. O. Gómez, R. L. Nydam, H. C. E. Larsson, M. S. Y. Lee, and M. W. Caldwell. 2019. New skulls and skeletons of the Cretaceous legged snake *Najash*, and the evolution of the modern snake body plan. Science Advances 5:1–9.

Gould, S. J. 1970. Dollo on Dollo's law: irreversibility and the status of evolutionary laws. Journal of the History of Biology 3:189–212.

Groth, J. G., and G. F. Barrowclough. 1999. Basal divergences in birds and the phylogenetic utility of the nuclear RAG-1 gene. Molecular Phylogenetics and Evolution 12:115–123.

Hall, R. 2002. Cenozoic geological and plate tectonic evolution of SE Asia and the SW Pacific: computer-based reconstructions, model and animations. Journal of Asian Earth Sciences 20:353–431.

Kearse, M., R. Moir, A. Wilson, S. Stones-Havas, M. Cheung, S. Sturrock, S. Buxton, A. Cooper, S. Markowitz, C. Duran, T. Thierer, B. Ashton, P. Meintjes, and A. Drummond. 2012. Geneious Basic: an integrated and extendable desktop software platform for the organization and analysis of sequence data. Bioinformatics 28: 1647–1649.

Keogh, J. S. 1998. Molecular phylogeny of elapid snakes and a consideration of their biogeographic history. Biological Journal of the Linnean Society 63:177–203.

Kocher, T. D., W. K. Thomas, A. Meyer, S. V. Edwards, S. Paabo, F. X. Villablanca, and A. C. Wilson. 1989. Dynamics of mitochondrial DNA evolution in animals: amplification and sequencing with conserved primers. Proceedings of the National Academy of Sciences of the United States of America 86:6196–6200.

Kraus, F. 2009. New species of *Toxicocalamus* (Squamata: Elapidae) from Papua New Guinea. Herpetologica 65:460–467.

———. 2017a. New species of blindsnakes (Squamata: Gerrhopilidae) from the offshore islands of Papua New Guinea. Zootaxa 4299:75–94.

———. 2017b. Two new species of *Toxicocalamus* (Squamata: Elapidae) from Papua New Guinea. Journal of Herpetology 51:574–581.

Kraus, F., and A. Allison. 2004. Two new treefrogs from Normanby Island, Papua New Guinea. Journal of Herpetology 38:197–207.

———. 2006. Three new species of *Cophixalus* (Anura: Microhylidae) from southeastern New Guinea. Herpetologica 62:202–220.

———. 2007. Taxonomic notes on frogs of the genus *Rana* from Milne Bay Province, Papua New Guinea. Herpetological Monographs 21: 33–75.

Lane, A., and R. Shine. 2011. Phylogenetic relationships within laticaudine sea snakes (Elapidae). Molecular Phylogenetics and Evolution 59:567–577.

Lanfear, R., P. B. Frandsen, A. M. Wright, T. Senfeld, and B. Calcott. 2017. PartitionFinder 2: new methods for selecting partitioned models of evolution for molecular and morphological phylogenetic analyses. Molecular Biology and Evolution 34:772–773.

Lavery, T. H., A. D. Olds, J. M. Seddon, and L. K. P. Leung. 2016. The mammals of northern Melanesia: speciation, ecology, and biogeography. Mammal Review 46:60–76.

Leaché, A. D., and M. K. Fujita. 2010. Bayesian species delimitation in West African forest geckos (*Hemidactylus fasciatus*). Proceedings of the Royal Society B: Biological Sciences 277:3071–3077.

Little, T. A., B. R. Hacker, S. M. Gordon, S. L. Baldwin, P. G. Fitzgerald, S. Ellis, and M. Korchinski. 2011. Diapiric exhumation of Earth's youngest (UHP) eclogites in the gneiss domes of the D'Entrecasteaux Islands, Papua New Guinea. Tectonophysics 510: 39–68.

Malnate, E. V., and G. Underwood. 1988. Australasian natricine snakes of the genus *Tropidonophis*. Proceedings of the Academy of Natural Sciences of Philadelphia 140:59–201.

Mayr, E., and J. M. Diamond. 2001. The Birds of Northern Melanesia: Speciation, Ecology and Biogeography. Oxford University Press, USA.

McDowell, S. B. 1969. *Toxicocalamus*, a New Guinea genus of snakes of the family Elapidae. Journal of Zoology 159:443–511.

McGuire, J. A., D. D. Cotoras, B. O'Connell, S. Z. S. Lawalata, C. Y. Wang-Claypool, A. Stubbs, X. Huang, G. O. U. Wogan, S. M. Hykin, S. B. Reilly, et al. 2018. Squeezing water from a stone: high-throughput sequencing from a 145-year old holotype resolves (barely) a cryptic species problem in flying lizards. PeerJ 2018:1–16.

Menzies, J. 2006. The Frogs of New Guinea and the Solomon Islands. Pensoft Publishers, Bulgaria.

Metzger, G. A., F. Kraus, A. Allison, and C. L. Parkinson. 2010. Uncovering cryptic diversity in *Aspidomorphus* (Serpentes: Elapidae): evidence from mitochondrial and nuclear markers. Molecular Phylogenetics and Evolution 54:405–416.

Mittermeier, R. A., C. G. Mittermeier, T. M. Brooks, J. D. Pilgrim, W. R. Konstant, G. A. B. da Fonseca, and C. Kormos. 2003. Wilderness and biodiversity conservation. Proceedings of the National Academy of Sciences of the United States of America 100:10309–10313.

O'Shea, M. 1996. A Guide to the Snakes of Papua New Guinea. Independent Publishing, Papua New Guinea.

O'Shea, M., F. Parker, and H. Kaiser. 2015. A new species of New Guinea worm-eating snake, genus *Toxicocalamus* (Serpentes: Elapidae), from the Star Mountains of Western Province, Papua New Guinea, with a revised dichotomous key to the genus. Bulletin of the Museum of Comparative Zoology 161:241–264.

O'Shea, M., A. Allison, and H. Kaiser. 2018. The taxonomic history of the enigmatic Papuan snake genus *Toxicocalamus* (Elapidae: Hydrophiinae), with the description of a new species from the Managalas Plateau of Oro Province, Papua New Guinea, and a revised dichotomous key. Amphibia Reptilia 39:403–433.

Palci, A., and M. W. Caldwell. 2013. Primary homologies of the circumorbital bones of snakes. Journal of Morphology 274:973–986.

Rambaut, A., A. J. Drummond, D. Xie, G. Baele, and M. A. Suchard. 2018. Posterior summarization in Bayesian phylogenetics using Tracer 1.7. Systematic Biology 67:901–904.

Rannala, B., and Z. Yang. 2003. Using DNA sequences from multiple loci. Genetics 1656:1645–1656.

Ronquist, F., and J. P. Huelsenbeck. 2003. MrBayes 3: Bayesian phylogenetic inference under mixed models. Bioinformatics 19: 1572–1574.

Rossman, C. E. 1980. Ontogenetic changes in skull proportions of the diamondback water snake, *Nerodia rhombifera*. Herpetologica 36:42–46.

Ruane, S., and C. C. Austin. 2017. Phylogenomics using formalin-fixed and 100+ year-old intractable natural history specimens. Molecular Ecology Resources 17:1003–1008.

Ruane, S., F. T. Burbrink, B. Randriamahatantsoa, and C. J. Raxworthy. 2016. The cat-eyed snakes of Madagascar: phylogeny and description of a new species of *Madagascarophis* (Serpentes: Lamprophiidae) from the Tsingy of Ankarana. Copeia 104:712–721.

Ruane, S., S. J. Richards, J. D. McVay, B. Tjaturadi, K. Krey, and C. C. Austin. 2018. Cryptic and non-cryptic diversity in New Guinea ground snakes of the genus *Stegonotus* Duméril, Bibron and Duméril, 1854: a description of four new species (Squamata: Colubridae). Journal of Natural History 52:917–944.

Sabaj, M. H. 2016. Standard symbolic codes for institutional resource collections in herpetology and ichthyology: an online reference. Version 6.5 [Internet]. Available from: http://www.asih.org/. Accessed 16 August 2016.

Saint, K. M., C. C. Austin, S. C. Donnellan, and M. N. Hutchinson. 1998. *C-mos*, a nuclear marker useful for squamate phylogenetic analysis. Molecular Phylogenetics and Evolution 10:259–263.

Sanders, K. L., M. S. Y. Lee, R. Leys, R. Foster, and J. Scott Keogh. 2008. Molecular phylogeny and divergence dates for Australasian elapids and sea snakes (Hydrophiinae): evidence from seven genes for rapid evolutionary radiations. Journal of Evolutionary Biology 21: 682–695.

Scanlon, J. D., and M. S. Y. Lee. 2004. Phylogeny of Australasian venomous snakes (Colubroidea, Elapidae, Hydrophiinae) based on phenotypic and molecular evidence. Zoologica Scripta 33:335–366.

SHINE, R., AND J. S. KEOGH. 1996. Food habits and reproductive biology of the endemic Melanesian elapids: are tropical snakes really different? Journal of Herpetology 30:238–247.

SIMMONS, J. E. 2015. Herpetological Collecting and Collections Management. Society for the Study of Amphibians and Reptiles, USA.

SLOWINSKI, J. B., J. BOUNDY, AND R. LAWSON. 2001. The phylogenetic relationships of Asian coral snakes (Elapidae: *Calliophis* and *Maticora*) based on morphological and molecular characters. Herpetologica 57: 233–245.

STAMATAKIS, A. 2014. RAxML version 8: a tool for phylogenetic analysis and post-analysis of large phylogenies. Bioinformatics 30:1312–1313.

STERNFELD, R. 1913. Beiträge zur Schlangenfauna NeuGuineas und der benachbarten Inselgruppen. Sitzungs-Berichte Der Gesellschaft Naturforschender Freunde Zu Berlin 1913:384–389.

STRICKLAND, J. L., S. CARTER, F. KRAUS, AND C. L. PARKINSON. 2016. Snake evolution in Melanesia: origin of the Hydrophiinae (Serpentes, Elapidae), and the evolutionary history of the enigmatic New Guinean elapid *Toxicocalamus*. Zoological Journal of the Linnean Society 178:663–678.

SUKUMARAN, J., AND L. L. KNOWLES. 2017. Multispecies coalescent delimits structure, not species. Proceedings of the National Academy of Sciences of the United States of America 114:1607–1611.

TAYLOR, B., A. GOODLIFFE, F. MARTINEZ, AND R. HEY. 1995. Continental rifting and initial sea-floor spreading in the Woodlark basin. Nature 374:534–537.

TAYLOR, B., A. M. GOODLIFFE, AND F. MARTINEZ. 1999. How continents break up: insights from Papua New Guinea. Journal of Geophysical Research: Solid Earth 104:7497–7512.

VAN UFFORD, A. Q., AND M. CLOOS. 2005. Cenozoic tectonics of New Guinea. American Association of Petroleum Geologists Bulletin 89: 119–140.

WEBB, L. E., S. L. BALDWIN, AND P. G. FITZGERALD. 2014. The Early-Middle Miocene subduction complex of the Louisiade Archipelago, southern margin of the Woodlark Rift. Geochemistry, Geophysics, Geosystems 15:4024–4046.

YANG, Z., AND B. RANNALA. 2010. Bayesian species delimitation using multilocus sequence data. Proceedings of the National Academy of Sciences of the United States of America 107:9264–9269.

Accepted: 6 October 2020.
Published online: 16 December 2020.

ZooBank ID: urn:lsid:zoobank.org:act:853F8768-BF06-4C73-A506-CFAC34336AD0

APPENDIX 1

Specimens Examined.—*Toxicocalamus ernstmayri*: Papua New Guinea: Western Province: Wangbin: Ok Tedi, 1,463 m (MCZ R-145946).

Toxicocalamus holopelturus: Papua New Guinea: Milne Bay Province (AMNH R-76660, holotype). Morphosource identifier (S45894).

Toxicocalamus loriae (clade 3): Papua New Guinea: Oro Province: Mt. Trafalgar (BPBM 39813, voucher). Oro Province: Collingwood Bay (LSUMZ 93563, voucher). Morphosource identifier (S23281).

Toxicocalamus mintoni: Papua New Guinea: Milne Bay Province: Sudest Island: western slope Mt. Rio, 400 m (BPBM 20822, holotype). Morphosource identifier (S45909).

Toxicocalamus misimae: Papua New Guinea: Milne Bay Province: Misima Island (AMNH R-76684, holotype). Morphosource identifier (S45892).

Toxicocalamus nigrescens: Papua New Guinea: Milne Bay Province: Fergusson Island: Oya Waka (BPBM 16545, holotype). Morphosource identifier (S45908).

Toxicocalamus pachysomus: Papua New Guinea: Milne Bay Province: along Upaelisafupi Stream, Cloudy Mountains (BPBM 15771, holotype). Morphosource identifier (S45907).

Toxicocalamus spilolepidotus: Papua New Guinea: Eastern Highlands Province (AMNH R-85745, holotype); Papua New Guinea: Eastern Highlands Province: Yaiya, Kratke Mountains (PNGNM 22132). Morphosource identifier (S45891).